Relaxation Techniques for Three-Dimensional Transonic Flow about Wings

F. R. BAILEY* AND J. L. STEGER†
NASA Ames Research Center, Moffett Field, Calif.

A relaxation procedure has been developed to treat the three-dimensional, transonic small-perturbation equations about finite lifting wings. A combination of two schemes is employed. For flow forward of the wing trailing edge the equations are written in terms of a velocity potential in order to minimize computer algebra and storage. For the remaining flowfield the equations are written in terms of the velocity components in order to simplify the enforcement of the Kutta condition. Difference equations and relaxation procedures are described for both schemes. The computational method automatically captures the embedded shock wave in the three-dimensional flowfield. Computed results agree with other inviscid methods and experiment.

Introduction

CURRENT numerical methods based on relaxation procedures have proven to be efficient techniques for the calculation of steady, two-dimensional irrotational transonic flow. Flow about airfoils has been treated by Murman and Cole,[1] Murman and Krupp,[2,3] and Steger and Lomax,[4,5] while Krupp and Murman,[3] and Bailey[6] have studied axisymmetric flow. With this established background one can begin the development of efficient procedures that will treat three-dimensional transonic flows about wings.

The extension of relaxation schemes to three dimensions generates a number of additional complications. A primary consideration is that computation time and computer storage requirements can increase by two orders of magnitude as the finite-difference network is extended to cover the third dimension. For these reasons the relaxation process must truly be efficient. Another consideration is that more complicated geometry makes the boundary conditions more difficult to apply. In particular, exact coordinate transformations, which have proven to be useful in two dimensions and which force the body to lie along the edge of a finite-difference network,[7,5] can be very difficult to apply to a complicated three-dimensional body. It is expected, however, that thin-wing boundary conditions are sufficiently accurate for a variety of interesting problems if one can overcome singularities inherent to thin-wing boundary conditions. The papers by Murman and Krupp, for example, have shown that some blunt-nosed airfoils are adequately modeled under the thin airfoil approximation by an appropriate choice of finite-difference schemes. Still additional complications arise when treating the finite lifting wing. In the case of a thin wing at small angles of attack, however, the treatment is greatly simplified by assuming the trailing vortex sheet lies in the plane of the wing.

In this paper we present relaxation methods for the solution of the three-dimensional small-disturbance transonic flow equations using both the velocity potential and the u, v, w velocity components. In the case of lifting wings, we depart from the previously reported methods used in lifting airfoil solutions.[3,5] Instead, we introduce an efficient hybrid relaxation procedure using both the velocity potential and velocity components themselves. The potential formulation is used upstream and over the major portion of the wing, while the velocity component formulation is used near the trailing edge and downstream in order to simplify the application of the Kutta condition.

Presented as Paper 72-189 at AIAA 10th Aerospace Sciences Meeting, January 17–19, San Diego, Calif.; submitted February 10, 1972; revision received October 6, 1972.
Index category: Subsonic and Transonic Flow.
* Research Scientist. Associate Member AIAA.
† Research Scientist. Member AIAA.

Transonic Small-Perturbation Equations

The nonlinear equations that describe inviscid, irrotational compressible flow can be simplified for slender-wing bodies. A suitable form when $M_\infty \to 1$ is derived by Spreiter[8] and may be written as

$$\left[(1-M_\infty{}^2)-\frac{(\gamma+1)M_\infty{}^2 u}{q_\infty}\right]\frac{\partial u}{\partial x}+\frac{\partial v}{\partial y}+\frac{\partial w}{\partial z}=0 \tag{1a}$$

$$\partial u/\partial z-\partial w/\partial x=0 \tag{1b}$$

$$\partial v/\partial z-\partial w/\partial y=0 \tag{1c}$$

for the Cartesian coordinate system defined along the wing by Fig. 1. Here u, v, w are perturbation velocity components in x, y, and z

$$u=q_x-q_\infty \tag{2a}$$

$$v=q_y \tag{2b}$$

$$w=q_z \tag{2c}$$

where q_x, q_y, and q_z are total-velocity components. At distances far from the body the flow is assumed to be uniform, aligned to the x axis, and of magnitude q_∞.

Considering the boundary conditions, the thin-wing tangency condition is given by

$$w=q_\infty[df(x,y,0)/dx-\alpha] \tag{3}$$

where $f(x,y,0)$ describes the shape of the wing and α is the angle of attack. Far from the wing and trailing vortex sheet u, v, and w are assumed to be zero. For lifting wings a Kutta condition must be imposed along the trailing edge of the wing so that

$$u_{\text{lower}}|_{TE}=u_{\text{upper}}|_{TE} \tag{4}$$

Provision is made in the downstream far field for a vortex

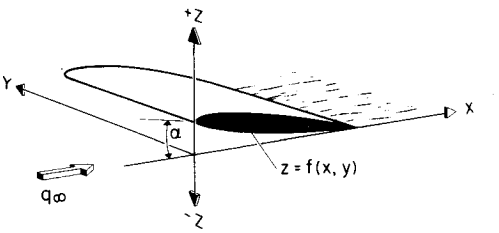

Fig. 1 Wing and coordinate system.

sheet trailing the wing. In particular, the velocity components v and w are left unspecified while u vanishes.

If a small-perturbation velocity potential is introduced

$$\partial\phi/\partial x = q_x - q_\infty \tag{5a}$$

$$\partial\phi/\partial y = q_y \tag{5b}$$

$$\partial\phi/\partial z = q_z \tag{5c}$$

Equations (1) assume the form

$$\left[(1-M_\infty{}^2)-(\gamma+1)\frac{M_\infty{}^2}{q_\infty}\frac{\partial\phi}{\partial x}\right]\frac{\partial^2\phi}{\partial x^2}+\frac{\partial^2\phi}{\partial y^2}+\frac{\partial^2\phi}{\partial z^2}=0 \tag{6}$$

The wing tangency boundary condition is given to first order by

$$\partial\phi/\partial z = q_\infty[df(x,y,0)/dx-\alpha] \tag{7}$$

and in the very far field away from the wing and trailing vortex sheet

$$\phi \to 0 \tag{8}$$

In order to bring the outer boundaries of the finite-difference mesh closer to the wing the numerical solution in the outer field is matched to an approximate analytic expression for the far field. Such a far field solution has been derived by Klunker[9] and contains contributions due to lift, wing thickness, and the nonlinearity of the transonic equation. The lift term decays like the reciprocal of the distance above and below the wing whereas the other two terms decay as the reciprocal of the square of the distance. Thus, only the lift term has been retained since it largely dominates the far-field solution. The contribution due to lift in regions far from the wing and trailing vortex sheet is given by

$$\phi_{\text{lift}} \simeq (1/4\pi)[z/(y^2+z^2)](1+x/R)\int_{S_w}\Delta u\, dS \tag{9}$$

where

$$R = [x^2+(1-M_\infty{}^2)(y^2+z^2)]^{1/2} \tag{10}$$

and S_w is the planform area. In the regon of the vortex sheet far downstream of the wing, the lift contribution must take into account the jump in potential across the sheet. An approximate expression for ϕ in this region is also given in Ref. 9, but is not required in this work.

Selection of Dependent Variables in Three-Dimensional Problems

Relaxation techniques to treat Eq. (6) in two dimensions have been developed primarily by Murman and his co-workers[1,2,3] and an efficient relaxation algorithm to treat Eq. (1) in two dimensions has been briefly indicated by Steger and Lomax.[4] The details of the latter scheme have remained largely unpublished in the general literature. Both techniques can be extended to three-dimensional problems and both techniques have about equal rates of convergence for a typical nonlifting problem. From the point of view of computer storage requirements and arithmetic—which can be crucial considerations in a three-dimensional problem—the velocity potential is a better choice of dependent variable than the values of u, v, w. At a given point in the finite-difference grid, Eqs. (1) require three times the storage of Eq. (6) and about $2 \to 2.5$ as much algebra per iteration step. (If the fully nonlinear irrotational equations are used, the ratio of arithmetic per step for the two methods drops sharply.) However, past experience with Eq. (6) in two dimensions shows that a typical lifting airfoil requires more iterations than a nonlifting profile. This situation arises because in a velocity potential formulation the circulation is an unknown magnitude which must be specified as part of the boundary conditions; and, generally, the circulation is found from an additional iteration process which is built onto the over-all relaxation procedure. In three dimensions the circulation varies in the spanwise direction and this further complicates the solution process.

Conversely, the Kutta condition is "naturally" imposed in a formulation using u, v, w as dependent variables. Equation (4) is simply enforced at the same time the airfoil boundary conditions are updated with each iteration of the field quantities. In the relaxation process the Kutta condition acts as a well-behaved boundary condition much as the tangency condition does, and the over-all rate of convergence is not significantly degraded in the lifting case. Unlike Eq. (6) the unknown magnitude of circulation does not enter into Eqs. (1) or its boundary conditions. Consequently, even though a formulation using the velocity components requires more algebra per step than the formulation using the velocity potential, one expects that for a typical lifting wing the method involving velocity components can have equivalent efficiency. Furthermore, relaxation procedures developed for the velocity components can possibly be extended to rotational flowfields.

Computer storage requirements—the other important consideration, since computer efficiency depends on data being in core or rapidly transferred into core—favor the velocity potential as the better choice of dependent variable. Moreover, singularities encountered in thin-wing theory such as at the leading edge are generally weaker in the velocity potential than in the velocity components. With these considerations in mind it appears that a practical approach to solving lifting problems is to use a combination of both Eqs. (1) and (6). In the present computational method Eq. (6) is used upstream from a station somewhat before the trailing edge of the wing; for example, up to and inclusive of the 90% chord station. Downstream from this juncture line Eqs. (1) are used and the Kutta condition is enforced in terms of the velocity components. In this manner storage requirements can be kept within more reasonable bounds.

In the remainder of this paper, differencing schemes and relaxation methods are described for both Eqs. (6) and (1). Some preliminary results illustrating the applicability of these schemes are described for a procedure using ϕ alone in the nonlifting case and a procedure comprised of ϕ and u, v, w in the lifting case.

Difference Equations

In selecting difference operators for Eqs. (1) and (6) we take note that because of their nonlinearity these equations encompass both subsonic and supersonic flow. A fundamental feature of transonic relaxation schemes is the use of central differencing for the x-derivatives when the flow is locally subsonic and upwind one-sided differencing for the x-derivatives when the flow is locally supersonic. The finite difference approximations for Eq. (6) and the associated boundary condition approximations are similar to those used in Refs. 1–3, 5, and 6, but are rewritten in the Appendix for an unequally spaced grid.

Due to the absence of second derivatives, the difference algorithms for Eq. (1) differ considerably from those for Eq. (6). In our treatment, operators were first selected to difference the dependent variables, u, v, and w, at grid points along the boundary edges. These operators as well as those required to couple Eqs. (1) and (6) at the juncture line are also described in the Appendix. For interior points all the derivatives in subsonic regions are differenced by operators which allow disturbances to travel in any direction. Difference operators which are interspersed to their data points and evaluated by an interpolation of the data are clearly suitable for y, z, and subsonic streamwise derivatives. We shall refer to such schemes as interpolative difference operators, and our main task is to select such operators for the first derivatives. Interpolative difference schemes require boundary conditions at each end of the finite-difference grid, and for this reason values of u, v, and w have been supplied along the edges of the grid by means of Eqs. (A8–A15).

To satisfy the above conditions, central differencing is used for x and y derivatives; but, for reasons that will be made clear later, an interchanging combination of backward-forward differencing is used for all z derivatives. The approximations selected for the z derivatives are second-order accurate and apply to unequally spaced grids. A typical term is written as

$$\left.\frac{\partial w}{\partial z}\right|_{j,k,l} = -C_0\cdot w_{j,k,l}+C_1\cdot w_{j,k,l+1}-C_2\cdot w_{j,k,l+2}$$

$$l = 2,4,6,\ldots,LM-2 \tag{11a}$$

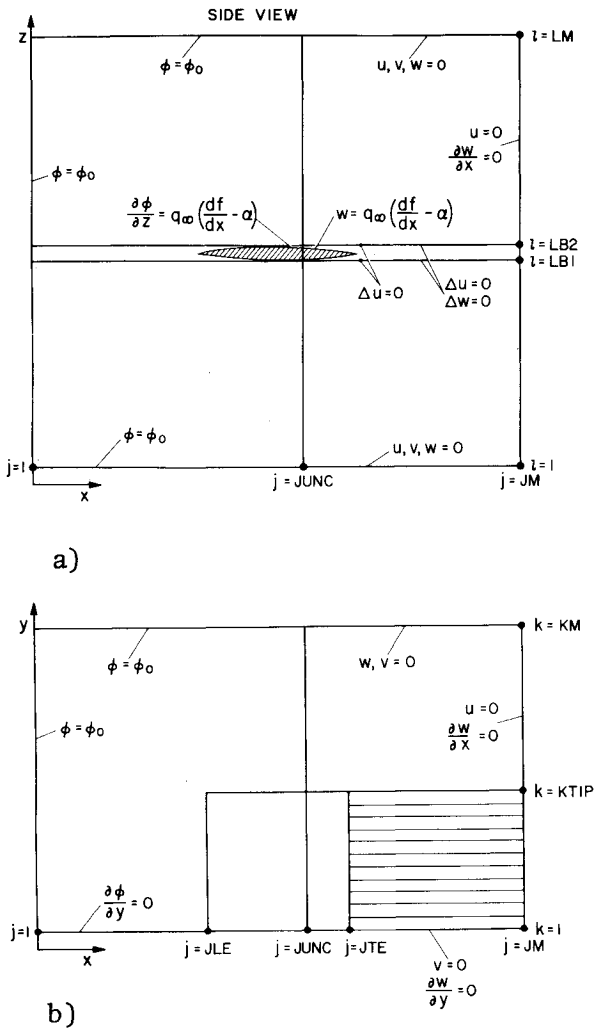

Fig. 2 Schematic of boundary conditions.

$$\left.\frac{\partial w}{\partial z}\right|_{j,k,l} = C_{0^-} w_{j,k,l} - C_{1^-} w_{j,k,l-1} + C_{2^-} w_{j,k,l-2}$$
$$l = 3, 5, 7, \ldots, LM-1 \qquad (11b)$$

where

$$C_{0^+} = C_{1^+} - C_{2^+}$$
$$C_{1^+} = (z_{l+2} - z_l)/(z_{l+1} - z_l)(z_{l+2} - z_{l+1})$$
$$C_{2^+} = (z_{l+1} - z_l)/(z_{l+2} - z_{l+1})(z_{l+2} - z_l)$$
$$C_{0^-} = C_{1^-} - C_{2^-}$$
$$C_{1^-} = (z_l - z_{l-2})/(z_l - z_{l-1})(z_{l-1} - z_{l-2})$$
$$C_{2^-} = (z_l - z_{l-1})/(z_{l-1} - z_{l-2})(z_l - z_{l-2})$$

and LM is the maximum number of grid points in z. LM and

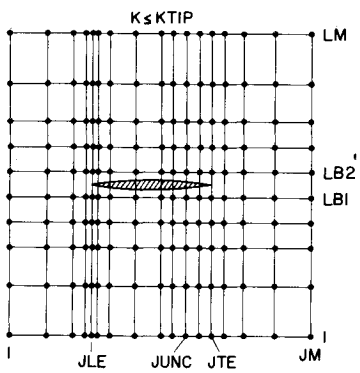

Fig. 3 $x-z$ plan view of grid.

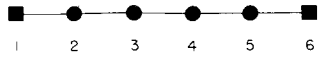

Fig. 4 Six-point line grid with end points.

$LB1$ are required to be even numbers (see Figs. 2 and 3), and values of w have been supplied at the end points $l = 1$, $LB1$, $LB2$, and LM.

The operator described in Eq. (11) is not conventional and thus requires some explanation. Note that the *upward* difference formula is used only at points which have an *even*-numbered l-index while the *downward* difference formula is used only at those points which have an *odd*-numbered l-index. This interchanging difference scheme fits within 2-point end conditions and every point along a z-grid line influences each and every other point along the same line. These properties are illustrated by an example in which $\partial w/\partial z$ is differenced along the uniformly spaced 6-point line grid of Fig. 4. Application of the operators generates the approximations

$$\frac{\partial}{\partial z}\begin{pmatrix} w_2 \\ w_3 \\ w_4 \\ w_5 \end{pmatrix} = \begin{pmatrix} -3 & 4 & -1 & 0 \\ -4 & 3 & 0 & 0 \\ 0 & 0 & -3 & 4 \\ 0 & 1 & -4 & 3 \end{pmatrix}\begin{pmatrix} w_2 \\ w_3 \\ w_4 \\ w_5 \end{pmatrix} + \begin{pmatrix} 0 \\ w_1 \\ -w_6 \\ 0 \end{pmatrix} \qquad (12)$$

for a uniform mesh, $\Delta z = 0.5$, and for specified end points w_1 and w_6. Both end conditions are employed in the approximation and from the matrix it is clear that the variables are fully coupled to each other—which is to say that the 4×4 matrix is irreducible.

The y-derivatives and the x-derivatives for subsonic regions have been differenced by a central operator identical to that used with $\partial\phi/\partial x$. The central operator also fits within single-point end conditions and also conveys information in both directions. However, unlike the interchanging difference operator, the centered difference operator does not couple adjacent points. The derivatives at even points are based solely on information at odd points, and the converse is true. This feature of central differencing can permit two disjoint smooth solutions as illustrated in Fig. 5. A well-known means of connecting every point of these data is to explicitly add second or fourth differences into the data. For example, the process of fitting 5 points by a least-squares parabola is equivalent to subtracting $-\frac{3}{35}$ of the fourth difference from each point (see, e.g., Lanczos,[11] p. 316). In this work a small fraction of the second difference is used to connect the functions in the x and y directions. Coupling terms such as

$$\delta_y(v_{j,k,l}) = \varepsilon(v_{j,k-1,l} - 2v_{j,k,l} + v_{j,k+1,l}) \qquad (13)$$

are explicitly added to the differenced analogs of Eqs. (1) but in an indirect fashion that we describe later. Here ε is kept small, $\varepsilon < 0(0.02)$.

In supersonic flow regions the absence of upstream propagation of disturbances is taken into account by replacing the x-derivatives by first-order accurate upwind operators such as

$$\left.\frac{\partial u}{\partial x}\right|_{j,k,l} = \frac{u_{j,k,l} - u_{j-2,k,l}}{x_j - x_{j-2}} \qquad (14)$$

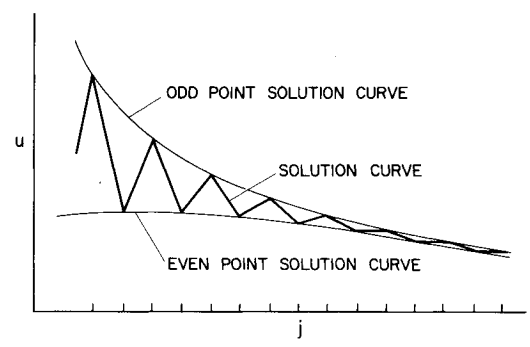

Fig. 5 Illustration of uncoupling of solution to central difference operator.

Like the central operator the upwind operator also does not properly couple one point to another. Thus, coupling terms similar to Eq. (13) but employing suitable upwind differencing are explicitly added.

In the transitions across the sonic-line from subsonic to supersonic flow and vice versa across the shock, it is desirable to avoid abrupt changes in the *evaluation* of the streamwise derivatives. Since the central difference operator is evaluated from different points than the upwind operator, it is unlikely that the two difference operators will give the same magnitude. Consequently, in order to avoid such abrupt changes, points in the vicinity of the sonic line or shock wave have been differenced by a blend of the operators according to the relation

$$\frac{\partial u}{\partial x} = b\frac{\partial u}{\partial x}\bigg|_{\text{central}} + (1-b)\frac{\partial u}{\partial x}\bigg|_{\text{upwind}} \tag{15}$$

where

$$b = 1-40[u/q_\infty - (1-M_\infty{}^2)/(\gamma+1)M_\infty{}^2]$$

and computer logic is used to constrain b to lie between 0 and 1.

Methods for Relaxation

Solutions to the difference equations that approximate both the velocity potential formulation and the velocity components formulation are obtained by the method of relaxation. In the case of the potential equation, Eq. (6), the relaxation procedure for two-dimensional flow has been described in detail in Refs. 1 and 6. The set of nonlinear algebraic equations formed by the difference approximations are solved by the method of successive line overrelaxation where all the points along a line in the z direction are inverted by the Gaussian elimination algorithm for tridiagonal matrices. During the course of the iteration process the velocity at each point is tested to determine whether the flow is locally subsonic or supersonic and the appropriate streamwise differencing is selected. In this way, shock waves, when they form, are permitted to evolve naturally. Numerical experimentation was used to estimate the optimum relaxation parameters to be just less than two for subsonic regions and just less than one for supersonic regions.

With the exception of the concept of using mixed elliptic-hyperbolic differencing for transonic flow, the differencing and iteration schemes used with Eq. (6) fall within the established theory of classical relaxation.[12,13] Classical relaxation procedures deal with the numerical differencing of a second derivative and much of their success stems from this difference analog. Thus, in linearized subsonic flow each second derivative operator generates symmetric, diagonally dominant, tridiagonal block matrices. Further, in linearized supersonic flow the upwind differencing of $\partial^2\phi/\partial x^2$ contributes only lower diagonal elements and the over-all matrix for the mixed flow is negative definite. Hence the simple Euler-predictor iteration scheme is stable for this matrix and acceleration devices such as successive overrelaxation simply act to improve the condition of the matrix.

In the sense described above, classical relaxation cannot be used with Eqs. (1) since only first-order derivatives appear. In linearized subsonic flow the central difference operator for a first derivative generates tridiagonal matrices that are neither diagonally dominant nor symmetric. Indeed, the central difference operators generate a matrix that is skew-symmetric with zero diagonal elements. The eigenvalues of this matrix are purely imaginary and the formulation is not convergent under most classical relaxation schemes—an exception being the method of steepest ascent (see, for example, Prozan[14]), which, unfortunately, is not a very efficient method. However, all relaxation techniques may be viewed as a subset of the theory for the numerical solution of ordinary differential equations;[15] and, to draw attention to this viewpoint we use the term "generalized relaxation."[4]

From the theory of generalized relaxation we have constructed several stable iteration procedures for the u, v, w difference equations previously described. Here we describe one of these procedures referred to as the interchange algorithm, which in this paper is presented without analysis.

To begin the description of the relaxation method we first define the difference analogs for Eqs. (1) as follows:

$$w'_{j,k,l} = \{[1-M_\infty{}^2-(\gamma+1)M_\infty{}^2(u/q_\infty)]\,\partial u/\partial x+\partial v/\partial y+\partial w/\partial z\}_{j,k,l} \tag{16a}$$

$$u'_{j,k,l} = \{\partial u/\partial z-\partial w/\partial x\}_{j,k,l} \tag{16b}$$

$$v'_{j,k,l} = \{\partial v/\partial z-\partial w/\partial y\}_{j,k,l} \tag{16c}$$

where $\{\ \}_{j,k,l}$ implies that the previously described difference operators have been applied. The prime superscript implies that a time-like difference operator is applied to the variable to establish an iteration sequence. Note that an iteration correspondence between w and Eq. (1a), u and Eq. (1b), and v and Eq. (1c) is established by Eqs. (16). In generalized relaxation methods such correspondence is arbitrarily selected, although the choice of correspondence is crucial to the convergence of a method.

The fundamental feature of the interchange algorithm is that pairs of points in the z direction are relaxed with their difference analogs interchanged. For example, the algorithm operates on Eq. (16) as follows:

$$w_{j,k,l}{}^{(n+1)} = w_{j,k,l}{}^{(n)} + w'_{j,k,l+1}{}^{(n,n+1)} + \tfrac{1}{2}[\delta_x{}^{(n,n+1)}(w_{j,k,l}) + \delta_y{}^{(n,n+1)}(w_{j,k,l})] \tag{17a}$$

$$w_{j,k,l+1}{}^{(n+1)} = w_{j,k,l+1}{}^{(n)} - w'_{j,k,l}{}^{(n,n+1)} + \tfrac{1}{2}[\delta_x{}^{(n,n+1)}(w_{j,k,l+1}) + \delta_y{}^{(n,n+1)}(w_{j,k,l+1})] \quad l = 2,4,6\ldots \tag{17b}$$

where the superscript (n) indicates the iteration time or count and the superscript $(n,n+1)$ implies that the most recently calculated points are used in the difference operators (in the sense of a Gauss-Siedel relaxation, for example). Note, that the coupling terms δ_x and δ_y described in Eq. (13) are included in the above algorithm but not interchanged.

Beginning with the interchange part of Eqs. (17), examination of the spatial subscripts indicates that the scheme has been constructed on the z-terms. Hence, the simplest way to view its operation is to apply it to the 4×4 matrix, Eq. (12), which was previously constructed for the z difference operators. The algorithm performs the following matrix multiplication on the matrix of Eq. (12):

$$\begin{pmatrix} \begin{pmatrix} 0 & 1 \\ -1 & 0 \end{pmatrix} & \begin{matrix} 0 & 0 \\ 0 & 0 \end{matrix} \\ \begin{matrix} 0 & 0 \\ 0 & 0 \end{matrix} & \begin{pmatrix} 0 & 1 \\ -1 & 0 \end{pmatrix} \end{pmatrix} \begin{pmatrix} -3 & 4 & -1 & 0 \\ -4 & 3 & 0 & 0 \\ 0 & 0 & -3 & 4 \\ 0 & 1 & -4 & 3 \end{pmatrix} = \begin{pmatrix} -4 & 3 & 0 & 0 \\ 3 & -4 & 1 & 0 \\ 0 & 1 & -4 & 3 \\ 0 & 0 & 3 & -4 \end{pmatrix} \tag{18}$$

In this case the algorithm takes a nearly skew symmetric matrix and converts it into a symmetric, diagonally dominant tridiagonal. The product matrix is negative definite and is stable under the usual iteration scheme defined by an Euler predictor. Furthermore, with the choice of the previously described difference operators for the x and y terms, the interchange algorithm works equally well for Eqs. (16). This is because for Eqs. (16) in linearized form only the elements due to the z differencing generate real eigenvalues. These remarks, of course, apply to points interior to the boundaries. The difference equations that correspond to differencing boundary points, for example Eq. (A9), are relaxed by a standard Gauss-Seidel technique.

Referring now to the coupling terms of Eqs. (17), it is clear from Eq. (13) that these terms generate negative definite tridiagonal matrices. Hence, these matrices enhance stability if they are added to the over-all matrix. For this reason the coupling terms are not made subject to the interchange and have been included with the difference equations that correspond to the variable being relaxed. It should be mentioned that only the term $\delta_x(u)$ is added to the approximation to Eq. (1b) and only the term $\delta_y(v)$ is added to the approximation to Eq. (1c). The approximations to Eq. (1) include the difference analogs given by Eq. (16) and the coupling terms; the sum of these terms comprise the residuals that are driven to zero.

The interchange algorithm applies not only to the 3-point forward-backward differencing, Eqs. (11), but also applies to

central formulas as well as interchanging combination of third-order accurate 4-point biased forward and 4-point biased backward differencing. All of these schemes fit within 2-point end conditions and when interchanged generate diagonally dominant block matrices; but only Eq. (11) has the advantage that the interchange algorithm brings the elements generated by z differencing into a tridiagonal form [Eq. (18) illustrated this property]. Consequently, the block matrices due to z differencing along a line of points can be inverted by the Gaussian elimination scheme for tridiagonals (the Thomas algorithm[16]). Hence, a successive line relaxation procedure can be written for the u, v, w equations just as it was for the ϕ equations. The line version of the u, v, w equations has convergence rates equivalent to the ϕ equations, but unlike the ϕ equations optimum relaxation parameters for u, v, w are strongly dependent on the ratios of the step sizes $(\Delta z/\Delta y)_{k,l}$ and $(\Delta z/\Delta x)_{j,l}$.

Results

Exploratory calculations have been performed using the perturbation potential for nonlifting cases and the hybrid $\phi-u$, v, w scheme for lifting cases. Solutions have been obtained for nontapered rectangular and sweptback wings of aspect ratios 2 and 4 with 6% thick circular arc airfoil sections. The wings did not have camber or twist although these features are easy to impose with thin-wing tangency conditions. With grid sizes of approximately 50 points in x and z and 20 points in y, the number of iterations required to obtain converged solutions ranged from 150 to 300 iterations with the corresponding computer time ranging from 30 to 60 min on an IBM 360/67. The number of iterations increased with increasing transonic effects and mesh refinement. It is interesting to note that the iterations count given above is of the same order as that required to obtain a comparable two-dimensional solution by the same techniques.

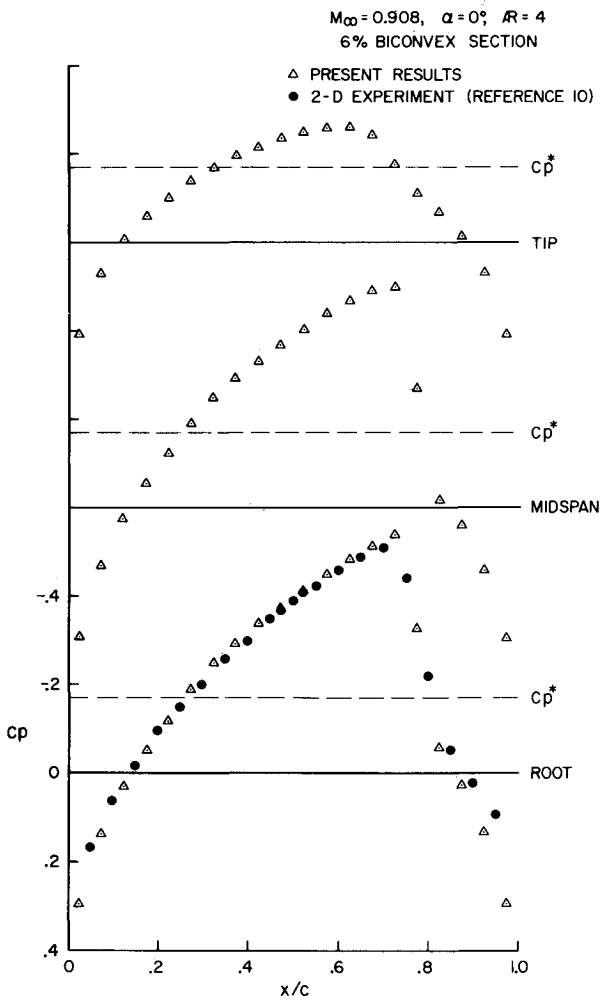

Fig. 6 Transonic C_p distribution on nonlifting rectangular wing.

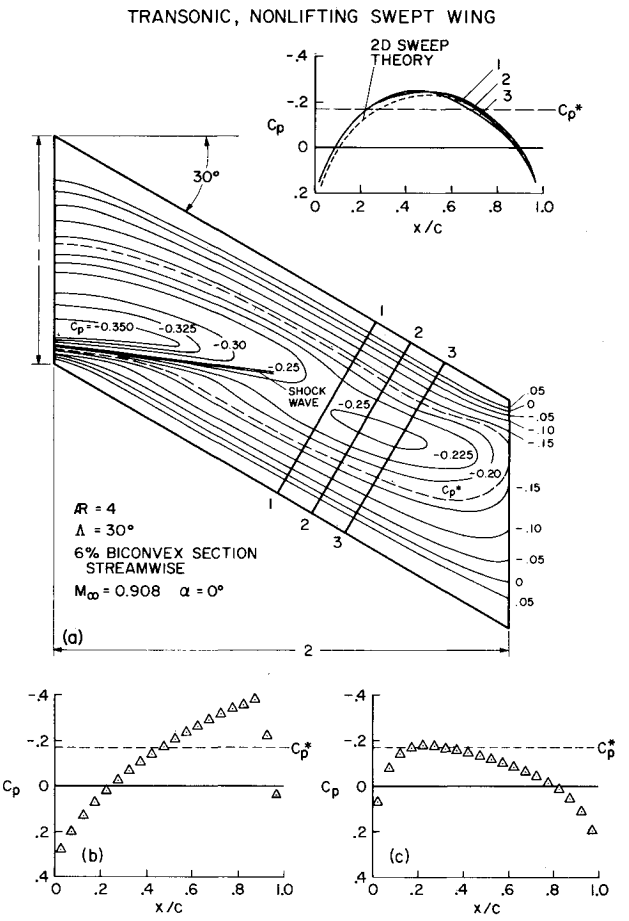

Fig. 7 Calculated pressures on transonic, nonlifting swept wing.

We first present results obtained using ϕ alone for a rectangular wing of aspect ratio 4, at zero angle of attack, and $M_\infty = 0.908$. Figure 6 displays the calculated pressure distribution at the root, midspan, and tip. At the root the calculated C_p distribution is shown to agree closely with the two-dimensional experimental data of Knechtel[10] for a circular arc profile of the same thickness ratio (6%). Note that the relief effect of the finite wing causes the embedded shock to weaken as one approaches the wing tip.

Some illustrative computations have also been made for a 30° sweptback wing with an aspect ratio 4 and with a 6% circular arc section placed parallel to the freestream. Figure 7a shows the calculated isobars on the wing surface and the chordwise pressure distributions at selected spanwise stations. The isobars are seen to coalesce and form an embedded shock near the trailing edge at the root station (see Fig. 7b). In contrast, the pressure distribution at the tip (Fig. 7c) is shockless and shows the minimum pressure peak occurring near the leading edge, as is characteristic of swept wings. It is interesting to note that supercritical shockless flow occurs over significant portions of the outboard sections. Near the $\frac{3}{4}$-span station the pressure contours are almost parallel to the leading and trailing edges, suggesting nearly two-dimensional flow in this region. The values of C_p along the three sections indicated are compared in Fig. 7(d) with a two-dimensional calculation at the Mach number and thickness ratio given by simple sweep theory. The comparison shows reasonable agreement between the finite-wing and two-dimensional results

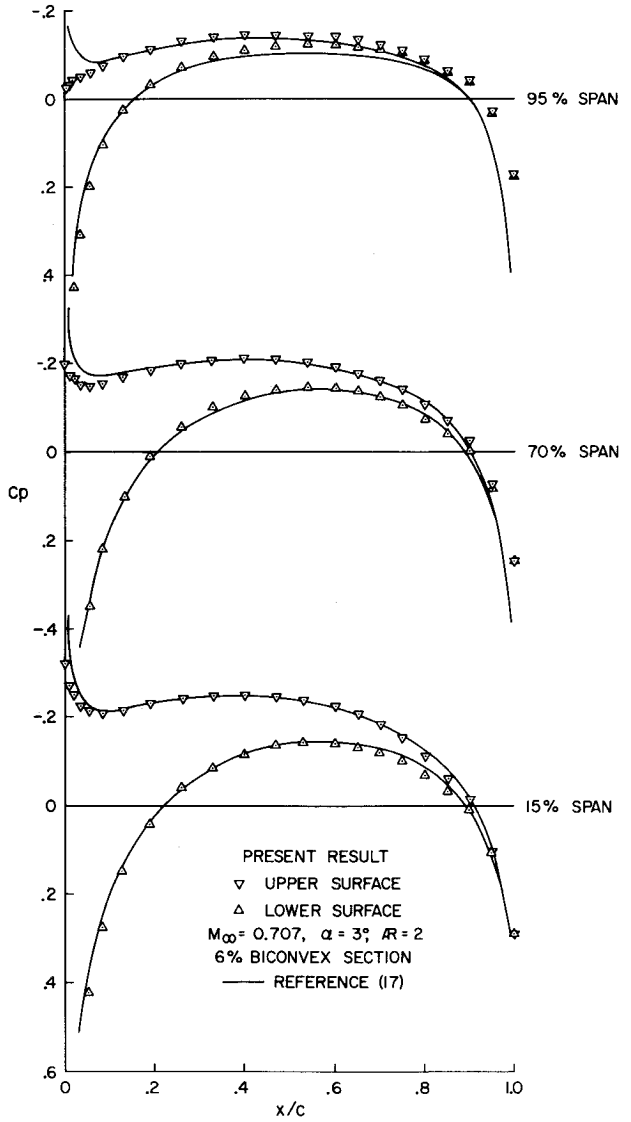

Fig. 8 Comparison with element method for subsonic lifting rectangular wing.

from sweep theory, although the former are shifted slightly upstream and show about 8% more expansion.

As an example of a listing case for a subsonic flowfield, Fig. 8 compares the pressure distribution calculated using the hybrid $\phi-u, v, w$ scheme with the linear results obtained from the computer program of Carmichael[17] which uses a distributed finite-element method. The wing is rectangular with aspect ratio = 2, $M_\infty = 0.707$, and $\alpha = 3°$. In this comparison the nonlinear terms of Eq. (6) were suppressed. The present results agree well with the element method except for some discrepancies at the leading edge and tip of the wing. These results were computed with the outer boundaries placed 2 chord-lengths upstream and downstream of the wing, 1 chord-length beyond the tip, and 3 chord-lengths above and below the wing. The calculations used the far field solution of Ref. 9 given in Eq. (9) and gave a lift coefficient of 0.1467, which is within 1% of the value 0.1476 obtained from the finite-element method. The same case run with the far field potential set to zero resulted in a 1% reduction in lift coefficient showing that the use of the analytical approximation of the far field was not of significant importance. However, when the upper and lower boundaries were placed at 1.8 chord-lengths the calculated lift using the analytical far field expression was 4% below the element method result, while that obtained with the potential set to zero in the far field was 11% below the value predicted by the element method. It is apparent in the present case that when the outer boundaries were sufficiently far removed so that the method gave good results using the far field solution, then equally good results are obtained by letting ϕ vanish.

An example of a lifting case for mixed subsonic-supersonic flow is shown in Fig. 9. Here the aspect ratio and angle of attack are the same as the previous case but with the Mach number increased to 0.885. The transonic effects are clearly evidenced by the presence of a shock on the upper wing surface at the root. This shock is seen to vanish as one proceeds toward the tip.

Finally, in Fig. 10 we present lifting results for supercritical flow over an aspect-ratio-4 wing at $M_\infty = 0.857$ and $\alpha = 1°$. The effect of tip relief is clearly illustrated in Fig. 10a. In addition, the coalescence of loading contours near the root indicates the presence of an embedded shock. The C_p distribution at the root (Fig. 10b) shows that this shock occurs only on the upper surface. The results here also show close agreement with the 2-D calculations, although 3-D relief effects are evident on the lower surface. At the 60% span station (Fig. 10c) the shock is considerably weakened and at the tip (Fig. 10d) the flow is completely subcritical.

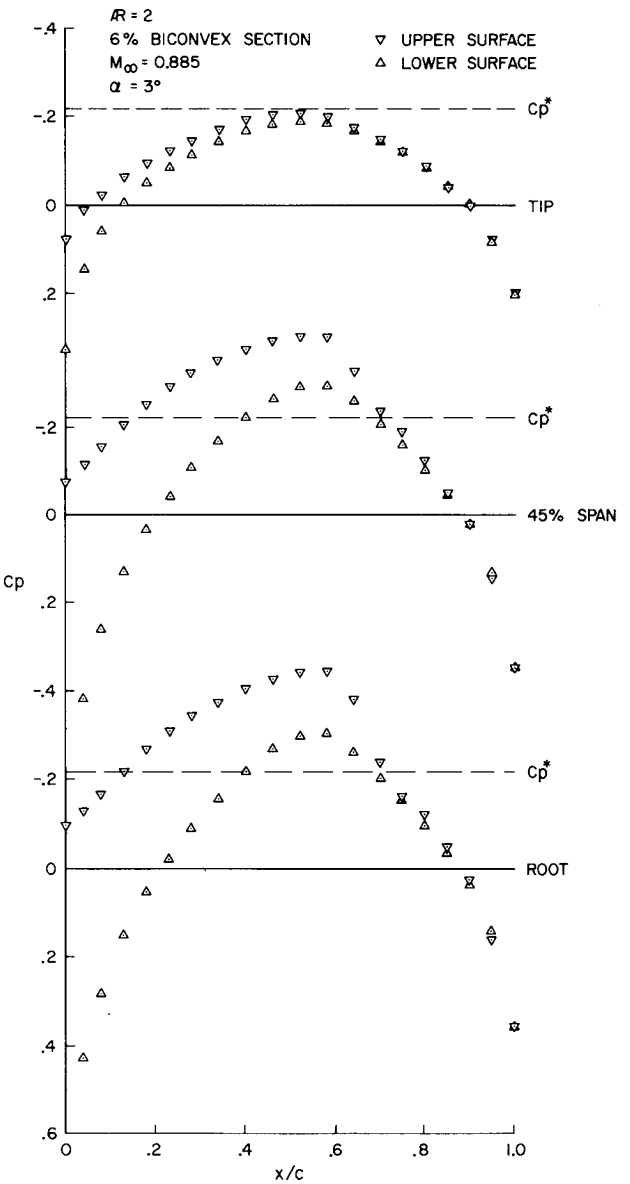

Fig. 9 Transonic C_p distribution on lifting rectangular wing.

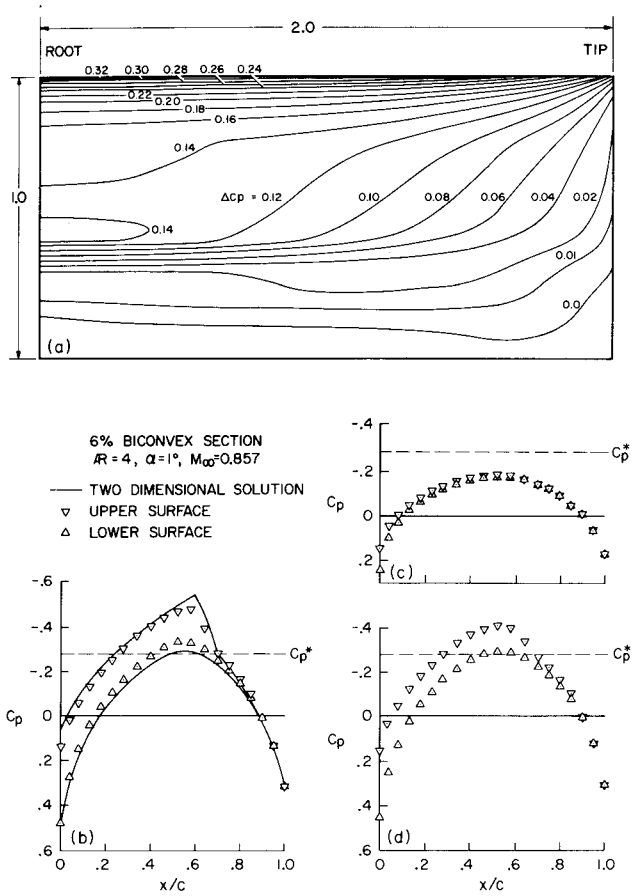

Fig. 10 Computed results for transonic lifting rectangular wing.

Appendix

A. Difference Equations and Boundary Conditions

Velocity potential differencing formulas

For subsonic flow the streamwise derivative approximations for an unequally spaced grid are given by

$$\partial\phi/\partial x|_{j,k,l} = A_1(\phi_{j-1,k,l}-\phi_{j,k,l})+A_2(\phi_{j+1,k,l}-\phi_{j,k,l}) \quad \text{(A1)}$$

$$\partial^2\phi/\partial x^2|_{j,k,l} = B_1(\phi_{j-1,k,l}-\phi_{j,k,l})+B_2(\phi_{j+1,k,l}-\phi_{j,k,l}) \quad \text{(A2)}$$

where

$$A_1 = (x_j-x_{j+1})/(x_j-x_{j-1})(x_{j+1}-x_{j-1})$$
$$A_2 = (x_j-x_{j-1})/(x_{j+1}-x_j)(x_{j+1}-x_{j-1})$$
$$B_1 = 2/(x_j-x_{j-1})(x_{j+1}-x_{j-1})$$
$$B_2 = 2/(x_{j+1}-x_j)(x_{j+1}-x_{j-1})$$

and the grid indices j, k, l correspond to the coordinates x, y, z. For supersonic flow the streamwise derivatives are approximated by

$$\partial\phi/\partial x|_{j,k,l} = (\phi_{j,k,l}-\phi_{j-2,k,l})/(x_j-x_{j-2}) \quad \text{(A3)}$$

$$\partial^2\phi/\partial x^2|_{j,k,l} = C_1(\phi_{j-2,k,l}-\phi_{j-1,k,l})+C_2(\phi_{j,k,l}-\phi_{j-1,k,l}) \quad \text{(A4)}$$

where

$$C_1 = 2/(x_{j-1}-x_{j-2})(x_j-x_{j-2}) \quad C_2 = 2/(x_j-x_{j-1})(x_j-x_{j-2})$$

The remaining derivatives, $\partial^2\phi/\partial y^2$ and $\partial^2\phi/\partial z^2$, are both central differenced in the manner of Eq. (A2). It should be noted that the central difference equations are first-order accurate when an unequally-spaced mesh is used and are second-order accurate for an equally-spaced mesh. The upwind differences, Eqs. (A3) and (A4) are always first-order accurate.

The tangency condition at the wing surface is satisfied at the boundary points $LB1$ and $LB2$ (see Figs. 2 and 3) by using the relation

$$\left.\frac{\partial^2\phi}{\partial z^2}\right|_{l=LB2} = \frac{1}{\Delta z}\left[\frac{\phi_{LB2+1}-\phi_{LB2}}{\Delta z} - q_\infty\frac{df(x,y,0^+)}{dx} - \alpha\right] \quad \text{(A5)}$$

for the upper wing surface and by a similar expression for the lower surface. As shown in Fig. 3 the planes $LB1$ and $LB2$ are placed half a mesh point off the wing plane and the next two vertical mesh spacings are equal.

Across the plane of the wing upstream of the leading edge and outboard of the tip ϕ must be continuous. This condition is insured by setting the potential at $LB1$ and $LB2$ equal to the midpoint value of ϕ interpolated from adjacent points above and below. Thus

$$\phi_{LB1} = \phi_{LB2} = \tfrac{9}{32}(\phi_{LB1-2}+\phi_{LB2+2})+\tfrac{25}{32}(\phi_{LB1-1}+\phi_{LB2+1}) \quad \text{(A6)}$$

This approximation was employed because the numerical method otherwise permitted a jump in $\partial\phi/\partial x$ across planes $LB1$ and $LB2$ in regions prior to the leading edge.

Along the plane $y = 0$ the symmetry condition is imposed by simply setting

$$\phi_{k=0} = \phi_{k=2} \quad \text{(A7)}$$

where the symmetry plane lies along $k = 1$.

Finally, the boundary conditions at the outer boundaries are approximated by letting ϕ vanish there or setting ϕ equal to the far field approximation given by Eq. (9).

The u, v, w difference equations at boundaries

The difference equations for interior points have been described in the text. The following relations are used to supply values of u, v, and w at each boundary surface.

Beginning with the interior boundaries, for conciseness of presentation we only describe difference equations for the upper surface, $LB2$, and write the operators as if the grid is uniform. The thin-wing tangency condition is imposed in the region JUNC $\leqq j \leqq JTE$ and $2 \leqq k \leqq$ KTIP, by the relation

$$\tfrac{3}{2}w_{j,k,LB2}-\tfrac{1}{2}w_{j,k,LB2+1} = q_\infty[df(x,y,+0)/dx-\alpha] \quad \text{(A8)}$$

which represents a linear extrapolation to the wing chord midway between $LB1$ and $LB2$. Values of u and v at these same points are supplied from the vorticity relations, Eqs. (1b and 1c), using upward differencing for z derivatives and central differencing for x and y derivatives. For example, u is found from the difference analog of Eq. (1b), which is

$$\frac{-3u_{j,k,LB2}+4u_{j,k,LB2+1}-u_{j,k,LB2+2}}{2\Delta z} - \frac{w_{j+1,k,LB2}-w_{j-1,k,LB2}}{2\Delta x} = 0 \quad \text{(A9)}$$

At the wing trailing edge the Kutta condition is imposed in the following manner: On the upper boundary plane, $LB2$, and u perturbation velocity is obtained from the vorticity relation, Eq. (A9). Along the lower boundary plane, however, the vorticity relation is replaced by the relation

$$u_{JTE,k,LB1} = u_{JTE,k,LB2} \quad \text{(A10)}$$

which assumes that the pressure is uniform between the planes $LB1$ and $LB2$.

Experience with two-dimensional calculations showed that the Kutta condition should be applied for at least several points off of the wing. Consequently, in three-dimensional calculations we have simply imposed the consistent thin-airfoil condition that u and w off the wing planform be uniform across the planes $LB1$ and $LB2$. This condition is satisfied by the following interpolation formula (written here for u only)

$$u_{j,k,LB1} = u_{j,k,LB2} = \tfrac{25}{32}(u_{j,k,LB1-1}+u_{j,k,LB2+1})-\tfrac{9}{32}(u_{j,k,LB1-2}+u_{j,k,LB2+2}) \quad \text{(A11)}$$

where the relation actually determines the value of u midway between $LB1$ and $LB2$.

Since v is not continuous across the trailing vortex sheet, values of v are supplied at $l = LB2$ and $LB1$ in the same manner as

along the wing planform. Equation (1c) is differenced at $LB2$ with second-order operators as follows

$$\frac{-3v_{j,k,LB2}+4v_{j,k,LB2+1}-v_{j,k,LB2+2}}{2\Delta z}=\frac{w_{j,k+1,LB2}-w_{j,k-1,LB2}}{2\Delta y} \tag{A12}$$

This differencing is always valid at any upper point in the flow and is used over the entire plane $LB2$.

Consider now the exterior boundaries. A uniform flow has been assumed in the far field; and u, v, and w are set to zero there except in the downstream far field plane, $j = JM$ (see Fig. 2). (To give u, v, and w along the far field boundaries is to overspecify the data at these points. However, the given data are consistent with the physical properties there and their constraint improves the rate of convergence of the relaxation method.) At the downstream far field plane, provision is made for a vortex sheet trailing from the finite wing. Along this plane u is set to zero, and

$$w_{JM,k,l} = w_{JM-1,k,l} \tag{A13}$$

which implies that in the far downstream w does not vary in x. It should be noted that no condition is placed on v, since values of v at $j = JM$ are not required by the interior differencing.

In the $x-z$ plane of symmetry, $k = 1$ in Fig. 2, $v = 0$, and $\partial u/\partial y$, $\partial w/\partial y = 0$. The latter condition ($u$ is not required) is satisfied by use of a simple second-order accurate forward difference operator

$$(1/2\Delta y)(-3w_{j,1,l}+4w_{j,2,l}-w_{j,3,l}) = 0 \tag{A14}$$

Finally, at the juncture, values of u and w are supplied by differencing ϕ, as we discuss in the next section.

B. Combining ϕ Equations with u, v, w

To combine the ϕ with the u, v, w equations the grids are simply overlapped at several points to permit disturbances to move from one grid region onto the other. The juncture line, $j = \text{JUNC}$ in Fig. 3, is the first interior point of the u, v, w equations and is the downstream boundary line for ϕ. Values of ϕ are obtained along this line by the identity

$$\partial\phi/\partial x = u$$

where $\partial\phi/\partial x$ is upwind differenced by the second-order accurate relation. Values of u, v, and w are supplied along the two planes JUNC-2, JUNC-1 by simply differencing ϕ. For subsonic flow, central difference operators are used; and, if the flow is supersonic, u is found by upwind differencing.

In practice we have found that the two methods stay everywhere compatible except near the tip of the finite lifting wing. At this singularity, the equations behave differently, the u, v, w being more sensitive. To keep the equations compatible, a simple averaging of u and w at the tip has been imposed. That is, at $k = KTIP$, $l = LB1$ and $LB2$, $\text{JUNC} \leq j \leq JTE$ (see Fig. 2), the averaging

$$u_{j,kl} = \tfrac{1}{2}(u_{j,k+1,l}+u_{j,k-1,l}) \tag{A15}$$

is used. A similar averaging has been used for u along the juncture on the wing, that is, at the points $l = LB1$ and $LB2$, $j = \text{JUNC}$, and $KTIP-1 \leq k \leq KTIP+1$. Two-dimensional solutions do not require such a fairing and it should be stressed that averaging is used only on the planes $LB1$ and $LB2$ in the vicinity of the wing tip.

References

[1] Murman, E. M. and Cole, J. D., "Calculation of Plane Steady Transonic Flows," *AIAA Journal*, Vol. 9, No. 1, Jan. 1971, pp. 114–121.

[2] Murman, E. M. and Krupp, J. A., "Solution of the Transonic Potential Equation Using a Mixed Finite Difference System," *Proceedings of the Second International Conference on Numerical Methods in Fluid Dynamics*, Vol. 8 of Lecture Notes in Physics, edited by M. Holt, Springer-Verlag, 1971, pp. 199–206.

[3] Krupp, J. A. and Murman, E. M., "The Numerical Calculation of Steady Transonic Flows Past Thin Lifting Airfoils and Slender Bodies," *AIAA Journal*, Vol. 10, No. 7, July 1972, pp. 880–886.

[4] Steger, J. L. and Lomax, H., "Generalized Relaxation Methods Applied to Problems in Transonic Flow," *Proceedings of the Second International Conference on Numerical Methods in Fluid Dynamics*. Vol. 8 of Lecture Notes in Physics, edited by M. Holt, Springer-Verlag, 1971, pp. 193–198.

[5] Steger, J. L. and Lomax, H., "Numerical Calculation of Transonic Flow About Two-Dimensional Airfoils by Relaxation Procedures," *AIAA Journal*, Vol. 10, No. 1, Jan. 1972, pp. 49–54.

[6] Bailey, F. R., "Numerical Calculation of Transonic Flow About Slender Bodies of Revolution," TN D-6582, 1971, NASA.

[7] Sells, C. C. L., "Plane Subcritical Flow Past a Lifting Aerofoil," TR 67146, June 1967, Royal Aircraft Establishment, England.

[8] Spreiter, J. R., "On the Application of Transonic Similarity Rules to Wings of Finite Span," Rept. 1153, 1953, NACA.

[9] Klunker, E. B., "Contribution to Methods for Calculating the Flow About Thin Lifting Wings at Transonic Speeds—Analytical Expression for the Far Field," TN D-6530, 1971, NASA.

[10] Knechtel, E. D., "Experimental Investigation at Transonic Speed of Pressure Distributions Over Wedge and Circular-Arc Airfoil Sections and Evaluation of Perforated-Wall Interference," TN D-15, 1959, NASA.

[11] Lanczos, C., *Applied Analysis*, Prentice-Hall, Englewood Cliffs, N.J.

[12] Varga, R. S., *Matrix Iterative Analysis*, Prentice-Hall, Englewood Cliffs, N.J., 1962.

[13] Wachspress, E. L., *Iterative Solution of Elliptic Systems*, Prentice-Hall, Englewood Cliffs, N.J., 1966.

[14] Prozan, R. J., "Transonic Flow in a Converging-Diverging Nozzle," Rept. LMSC/HREC D162177, NASA Contract NAS7-743, 1970, Lockheed Missiles & Space Co., Huntsville, Ala.

[15] Lomax, H., "An Operational Unification of Finite Difference Methods for the Numerical Integration of Ordinary Differential Equations," TR R-262, 1967, NASA.

[16] Ames, W. F., *Numerical Methods for Partial Differential Equations*," Barnes and Noble, New York, 1969.

[17] Carmichael, R. L., Castellane, C. R., and Chen, C. F., *The Use of Finite Element Methods for Predicting the Aerodynamics of Wing-Body Combinations in Analytic Methods in Aircraft Aerodynamics*, NASA SP-228, 1970.